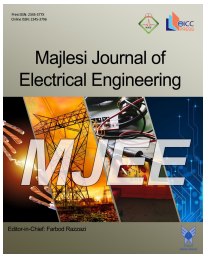

Majlesi J. Electr. Eng. 2026; 20(1) : 57-72

Majlesi Journal of Electrical Engineering (MJEE)

https://dx.doi.org/10.57647/mjee.2026.2001.05

Original Research

Adaptive Control of Freedom Upper-Limb Exoskeleton Robots Using Extreme Learning Machine and Terminal Sliding Mode

Morteza Mirzaee*, Reza Kazemi

Faculty of Mechanical Engineering, K.N. Toosi University of Technology, Tehran, Iran

***Corresponding author:** mortezamirzaee@email.kntu.ac.ir

Article History

Received:
6 November 2024

Revised:
4 February 2025

Accepted:
1 March 2025

Published in Issue:
31 March 2026

Abstract:

This paper presents a novel Adaptive Dynamic Terminal Sliding Mode Controller (ADTSMC) with an exponential reaching law, specifically designed for precise position control of 5-Degree of Freedom (DOF) upper-limb exoskeleton robots. The proposed control strategy addresses critical challenges in precision, stability, and adaptability, introducing several key innovations. Firstly, the incorporation of a Terminal Sliding Mode Surface (TSMS) ensures finite-time convergence of system states, significantly enhancing tracking performance. Secondly, the integration of Dynamic Second-Order Sliding Mode Control (DSMC) with an exponential reaching law mitigates chattering, providing smoother and more reliable control inputs. Thirdly, an Extreme Learning Machine (ELM) is utilized to optimize controller parameters in real-time, offering robustness against uncertainties and variations in system dynamics while managing the complex nonlinearities of upper-limb exoskeletons. The ELM helps maintain stable learning and avoids issues such as gradient vanishing. The stability of the closed-loop system is rigorously validated using a Lyapunov candidate function, ensuring reliable operation under varying conditions. Simulation results show that the proposed adaptive DSMC outperforms existing methods in terms of convergence speed, tracking accuracy, and chattering suppression, demonstrating a significant improvement in performance, with reductions of approximately 74.3% in performance indices.

Keywords: Exoskeleton robot; Sliding Mode Control; Neural network; Adaptive control; Rehabilitation robotics

Cite this article: Mirzaee M, Kazemi R. Adaptive Control of Freedom Upper-Limb Exoskeleton Robots Using Extreme Learning Machine and Terminal Sliding Mode. Majlesi J. Electr. Eng. 2026;20(1): 57-72. https://dx.doi.org/10.57647/mjee.2026.2001.05

1. Introduction

Upper-limb exoskeleton robots, particularly those with a 5-DOF configuration, have garnered significant attention for their potential to aid in rehabilitation and support elderly or disabled individuals [1]. These robots enable users to perform precise arm and body movements along desired trajectories, making them invaluable for improving mobility and independence. However, controlling such robots is inherently challenging due to system nonlinearity, uncertainties in dynamics, and the complexity of managing multiple inputs and outputs. These challenges are further intensified by the need for stability, adaptability to dynamic environments, and responsiveness to varying user conditions [2]. Effective control is crucial to address these complexities, ensuring the robot operates harmoniously with the user's intentions while mimicking natural arm motion. This is especially important in rehabilitation, where accurate and adaptive control can significantly enhance outcomes such as improved muscle strength, range of motion, and motor coordination. Vaziri and Fang propose an optimal inferential control framework for convolutional neural networks, addressing the challenge of controlling complex spatio-temporal systems by transforming the control problem into a probabilistic inference task [3].

Various control strategies have been proposed for the trajectory control of 5-DOF upper-limb exoskeleton robots. Sliding Mode Control (SMC) is widely used due

to its robustness in managing external disruptions, nonlinearities, and uncertainties, ensuring fast and dynamic responses for precise trajectory tracking. However, SMC faces a major limitation in the form of chattering, which can cause instability and performance degradation [4]. To address this, Dynamic Sliding Mode Control (DSMC) has been introduced as a higher-order variant of SMC, incorporating two sliding surfaces to effectively suppress chattering, resulting in smoother control signals and improved system stability [5]. Cooperative deterministic learning-based formation control for nonlinear mechanical systems under complete uncertainty involves using artificial neural networks to enhance distributed learning and knowledge consensus, enabling these systems to track complex formations despite uncertain dynamics [6]. This work enhances precision in sustained visual attention training by fine-tuning classifiers through offline EEG signal analysis. Techniques like SVM and RF models are used to decode attentional states, achieving notable accuracy and AUC values, thereby improving system efficacy [7].

The conventional SMC approach struggles with ensuring finite-time convergence. To overcome this, Terminal Sliding Mode Control (TSMC) was developed, addressing infinite settling time and ensuring finite-time convergence [8]. Additionally, TSMC enhances the system's convergence rate, providing the dual benefits of faster convergence and guaranteed finite-time state achievement [9, 10]. This paper presents a finite-time continuous terminal sliding mode control strategy for servo motor systems, which can achieve fast and precise tracking control, and guarantee finite-time convergence and robustness against uncertainties and disturbances. Babaey and Ravindran propose GenSQLi, a generative AI framework leveraging large language models to automatically create and evolve Web Application Firewall rules for defending against SQL injection attacks [11]. Babaey and Ravindran propose GenXSS, an AI-driven framework that automatically generates and validates sophisticated XSS attack payloads to test and improve web application firewall defenses [12]. Nasri et al. explore using eye-tracking data combined with machine learning to detect cognitive load during complex virtual reality training tasks, demonstrating the feasibility of predicting cognitive load through pupil dilation and fixation duration [13]. This paper introduces an adaptive control strategy for spur gear systems using proximal policy optimization and attention-based learning, aiming to improve system performance and fault tolerance under varying operational conditions [14]. This paper proposes a composite distributed learning approach for nonlinear multi-agent systems with uncertain dynamics, enabling synchronization through adaptive control and parameter estimation. The method ensures convergence and stability without requiring prior knowledge of the agents' dynamics [15]. This paper presents an adaptive formation learning control strategy for cooperative autonomous underwater vehicles operating under complete uncertainty, ensuring precise formation tracking without prior knowledge of system dynamics. The approach combines adaptive control with iterative learning to improve performance over repeated tasks [16].

The efficacy of the conventional SMC strategy depends heavily on its parameter values, making the task of obtaining these parameters a key challenge. To address this, intelligent systems like fuzzy logic and neural networks have emerged as promising solutions. These methods optimize controller parameters, improving the performance and adaptability of the SMC strategy. An adaptive intelligent controller can also enhance robustness against uncertainties and external disturbances. Conventional neural network controllers face challenges like local optima, slow convergence, and high time consumption. To overcome these issues, the Extreme Learning Machine (ELM) neural network was introduced, offering a solution for real-time control applications. ELM uses a single hidden layer and has been applied in various fields, including control, synchronization, and identification [17]. Nasri et al. present a virtual reality training apprenticeship for teaching novices the complex process of cold spray advanced manufacturing, offering a step-by-step training solution that addresses the spatial and procedural learning requirements of this technology [18]. Vaziri, Askari, and Fang propose Bayesian Inferential Motion Planning (BIMP) enhanced by heavy-tailed distributions, specifically Student's-t distributions, to improve probabilistic search efficiency and explore low-probability regions in motion planning [19]. Ghajari et al. propose a hyperdimensional computing framework for intrusion detection in IoT networks using the NSL-KDD dataset, achieving a high accuracy in identifying and classifying various attack types and normal traffic [20]. Ghajari et al. propose a novel network anomaly detection approach using HDC techniques on the NSL-KDD dataset, achieving an accuracy of 91.55% on the KDDTrain+ subset [21]. This paper evaluates the accuracy and reliability of statistical forecasting and predictive intelligence methods using a stochastic dataset, highlighting their effectiveness in handling uncertainty and variability in advanced manufacturing applications [22]. This paper proposes an adaptive-intelligent controller for quadcopters based on brain emotional learning, aiming to enhance stability and performance in the presence of uncertainties and nonlinearities [23]. This paper compares the effectiveness of multilayer perceptron (MLP) neural networks and logistic regression in modeling sustainability determinants, highlighting the superior performance of MLP in handling complex, nonlinear relationships [24]. This paper presents a deep learning-based method for automated detection of microcracks in second harmonic generation images of cartilage, improving the accuracy and efficiency of early osteoarthritis diagnosis [25]. This paper explores the role of artificial intelligence and machine learning in optimizing supply chain operations, emphasizing their ability to enhance demand forecasting, inventory management, and logistics planning [26].

Building on previous research, this study introduces a novel Adaptive Dynamic Terminal Sliding Mode Con-

https://dx.doi.org/10.57647/mjee.2026.2001.05

troller (ADTSMC) with an exponential reaching law, specifically tailored for the position control of 5-DOF upper-limb exoskeleton robots. The key contributions of the proposed method are as follows:

- **Terminal Sliding Mode Surface for Finite-Time Convergence:** A TSMS is proposed to achieve finite-time convergence of the system states. This innovation ensures that the system trajectories are guided toward the desired states within a predefined time frame, significantly enhancing tracking accuracy and responsiveness.

- **Dynamic Second-Order Sliding Mode Control with Exponential Reaching Law:** The controller integrates DSMC with a novel exponential reaching law to address chattering phenomenon. This innovation ensures smoother control inputs and improved system stability, reducing mechanical wear and enhancing the reliability of robot operations.

- **Adaptive Control through ELM:** The incorporation of the ELM neural network enables real-time adaptation by learning and optimizing controller parameters dynamically. This direct adaptive mechanism ensures robustness and adaptability in the face of uncertainties and varying operating conditions, a critical advancement for practical applications.

- **Addressing Complex Dynamics with ELM Neural Network:** The proposed strategy leverages the ELM network to effectively model and compensate for the intricate nonlinear dynamics of the 5-DOF upper-limb exoskeleton. By avoiding challenges such as gradient vanishing in traditional neural networks, the ELM provides a stable and efficient learning process, ensuring precise control under complex scenarios.

These contributions mark a significant step forward in adaptive control strategies for upper-limb exoskeleton robots, focusing on robustness, stability, and precision in dynamic and unpredictable environments. The proposed control strategy effectively addresses key challenges in exoskeleton robot control, such as convergence, stability, adaptability, and the handling of complex dynamics. The performance of the strategy is validated through two simulation scenarios, where it outperforms other position control methods. Additionally, a comparison with the SMC integrated with Fuzzy Neural Networks (FNN), as proposed in [27], demonstrates the superiority of the proposed method, highlighting its improved performance and reliability for practical use.

The organization of this paper is as follows. Section 2, describes the dynamic model of 5-DOF upper-limb exoskeleton robot. Section 3 presented the proposed control strategy. Section 4 presents various simulation scenarios, and the study's findings are summarized in the concluding Section 5.

2. Method

2.1 System description

This section derives the dynamic model of the 5-DOF exoskeleton robot, providing a detailed explanation of the equations through both Lagrange and state-space formulations. The 5-DOF upper-limb exoskeleton robot consists of a series of interconnected links and joints, which work together to enable movement in different directions. The robot has 5 links, each representing a DOF, and these links are connected by joints that allow for movement between them. Each joint has a specific range of motion, which enables the robot to move in a specific way, providing a range of motion that allows the robot to perform various tasks. Equation (1) represents the exoskeleton robot using Lagrange equations, which are formulated based on [28].

$$\boldsymbol{M}(\boldsymbol{q})\ddot{\boldsymbol{q}} + \boldsymbol{C}(\boldsymbol{q},\dot{\boldsymbol{q}})\dot{\boldsymbol{q}} + \boldsymbol{g}(\boldsymbol{q}) + \boldsymbol{J}^T(\boldsymbol{q})\boldsymbol{f} = \boldsymbol{\tau} \quad (1)$$

where $\boldsymbol{q}$, $\dot{\boldsymbol{q}}$, $\ddot{\boldsymbol{q}} \in \boldsymbol{R}^5$ represents the position, velocity, and acceleration vectors of the robot, respectively, $\boldsymbol{\tau}$ are the torque inputs and external disturbances, $\boldsymbol{J}$ is the Jacobian matrix, $\boldsymbol{f}$ is the input disturbance, $\boldsymbol{M}(\boldsymbol{q})$ denotes the inertia matrix, $\boldsymbol{C}(\boldsymbol{q},\dot{\boldsymbol{q}})$ is the coriolis and centripetal matrix, and $\boldsymbol{g}(\boldsymbol{q})$ is the gravity vector. The more information about the $\boldsymbol{M}(\boldsymbol{q})$,$\boldsymbol{C}(\boldsymbol{q},\dot{\boldsymbol{q}})$, $\boldsymbol{g}(\boldsymbol{q})$ and the nominal inertial and gravitational constant parameters are presented in [28]. Equation (1) is reformulated by letting $\boldsymbol{x_1}$ and $\boldsymbol{x_2}$ represent $\boldsymbol{q}$ and $\dot{\boldsymbol{q}}$, yielding equation (2).

$$\boldsymbol{M}(\boldsymbol{x_1})\dot{\boldsymbol{x}}_2 + \boldsymbol{C}(\boldsymbol{x_1},\boldsymbol{x_2})\boldsymbol{x_2} + \boldsymbol{g}(\boldsymbol{x_1}) + \boldsymbol{J}^T(\boldsymbol{x_1},\boldsymbol{x_2})\boldsymbol{f} = \boldsymbol{u} \quad (2)$$

In this equation, $\boldsymbol{f}$ represents the external disturbance, and $\boldsymbol{u}$ represents the control input. According to (2), the state space of the robot is transformed to state space model

$$\begin{aligned} \dot{\boldsymbol{x}}_1 &= \boldsymbol{x_2} \\ \dot{\boldsymbol{x}}_2 &= F + G\boldsymbol{u} \quad x = [x_1, x_2, x_3, x_4, x_5]^T \end{aligned} \quad (3)$$

F = $-\boldsymbol{M}^{-1}(\boldsymbol{x_1})[\boldsymbol{C}(\boldsymbol{x_1},\boldsymbol{x_2})\boldsymbol{x_2} + \boldsymbol{g}(\boldsymbol{x_1}) + \boldsymbol{J}^T\boldsymbol{f}]$ and G = $-\boldsymbol{M}^{-1}(\boldsymbol{x_1})$. To facilitate a clearer understanding of the dynamic model described in equation (3), the following assumptions are made.

Assumption 1: All state vectors are assumed measurable, obtainable from sensors, and twice differentiable, ensuring continuous first and second derivatives essential for control laws based on velocity and acceleration.

Assumption 2: The external disturbance i.e., $\boldsymbol{f}$ is a low frequency and bounded signal.

Assumption 2 states that the external disturbance, denoted as $\boldsymbol{f}$, is a low-frequency and bounded signal. This assumption is grounded in practical scenarios and system constraints, considering the impact of disturbances on system dynamics. "Low frequency" implies that disturbances vary at a rate significantly lower than the system's operational bandwidth, focusing on dominant influences. The term "bounded" emphasizes limitations on disturbance amplitude, crucial for stability, given

https://dx.doi.org/10.57647/mjee.2026.2001.05

that disturbances primarily arise from user forces and human-robot interactions.

The disturbances primarily originate from forces applied by the human operator, capturing the dynamic and unpredictable nature of human-robot interactions. The disturbance signal's nature closely mimics variations in human-applied forces, aligning with the study's commitment to authenticity. Figure 1 illustrates the schematic diagram of the 5-DOF upper-limb exoskeleton robot [28].

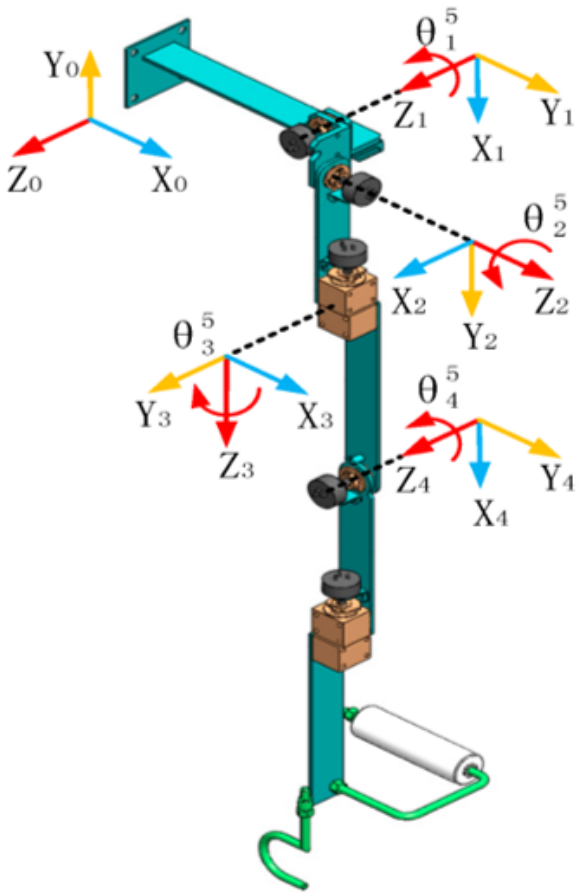

Figure 1. Schematic of the 5-DOF upper-limb exoskeleton robot.

2.2 DTSMC controller

The desired output i.e., the desired state vector is defined as $\boldsymbol{x_d} = [x_{1d}, x_{2d}, x_{3d}, x_{4d}, x_{5d}]^T$; as a result, the tracking error is defined as

$$\begin{aligned} &\widetilde{\boldsymbol{x}} = \boldsymbol{x} - \boldsymbol{x_d} \\ &\widetilde{\boldsymbol{x_1}} = [(x_1 - x_{1d}), (x_2 - x_{2d}), (x_3 - x_{3d}), (x_4 - x_{4d}), \\ &(x_5 - x_{5d}),]^T = [\widetilde{x}_1, \widetilde{x}_2, \widetilde{x}_3, \widetilde{x}_4, \widetilde{x}_5]^T \\ &\dot{\widetilde{\boldsymbol{x}}}_{\boldsymbol{2}} = F + G\boldsymbol{u} - \dot{\boldsymbol{x}}_{\boldsymbol{2d}} \end{aligned} \tag{4}$$

where $\tilde{x}$ denotes the tracking error vector. Based on assumption $(1-2)$, the derivative of (4) is achieved as

$$\begin{aligned} \ddot{\boldsymbol{x}}_{\boldsymbol{2}} &= \dot{F} + G\dot{\boldsymbol{u}} + \dot{G}\boldsymbol{u} \\ \ddot{\widetilde{\boldsymbol{x}}}_{\boldsymbol{2}} &= \ddot{\boldsymbol{x}}_{\boldsymbol{2}} - \ddot{\boldsymbol{x}}_{\boldsymbol{2d}} = \dot{F} + G\dot{\boldsymbol{u}} + \dot{G}\boldsymbol{u} - \ddot{\boldsymbol{x}}_{\boldsymbol{2d}} \end{aligned} \tag{5}$$

DTSMC sliding surfaces are introduces in (6)-(7).

$$\boldsymbol{s} = \dot{\widetilde{\boldsymbol{x}}}_{\boldsymbol{2}} + \alpha_1 \widetilde{\boldsymbol{x}}_{\boldsymbol{1}} \qquad \alpha_1 > 0, \quad \boldsymbol{s} \in \mathbb{R}^5 \tag{6}$$

$$\boldsymbol{\sigma} = \dot{\boldsymbol{s}} + \alpha_2 |\boldsymbol{s}|^{\gamma} \mathrm{sign}(\boldsymbol{s}) \quad \alpha_2 > 0, \quad 0 < \gamma < 2, \quad \boldsymbol{\sigma} \in \mathbb{R}^5 \tag{7}$$

where $\boldsymbol{s}$ and $\boldsymbol{\sigma} \in \boldsymbol{R}^5$ are the first and secondary 5-dimensional DTSMC sliding surface vectors, respectively, and α_1, α_2, and γ_1 are the nominal parameters.

Remark 1: Within equations (6)-(7), these three parameters encompassing α_1, α_2, γ wield significant influence over critical facets of the DTSMC surfaces. These parameters intricately impact the convergence rate, the attenuation of chattering, and the overall stability of the system.

Manifestly, the temporal derivatives of the DTSMC surfaces are elegantly expressed as follows:

$$\dot{\boldsymbol{s}} = \ddot{\widetilde{\boldsymbol{x}}}_{\boldsymbol{2}} + \alpha_1 \dot{\widetilde{\boldsymbol{x}}}_{\boldsymbol{2}}, \tag{8}$$

$$\dot{\boldsymbol{\sigma}} = \ddot{\boldsymbol{s}} + \alpha_2 \gamma |\boldsymbol{s}|^{\gamma-1} \dot{\boldsymbol{s}} \tag{9}$$

the second derivative of (9) is represented for implement of DTSMC surfaces as

$$\ddot{\boldsymbol{s}} = \dddot{\widetilde{\boldsymbol{x}}}_{\boldsymbol{2}} + \alpha_1 \ddot{\widetilde{\boldsymbol{x}}}_{\boldsymbol{2}} \tag{10}$$

using (10), the derivative of the secondary DTSMC sliding surfaces is presented as

$$\dot{\boldsymbol{\sigma}} = \ddot{\boldsymbol{s}} + \alpha_2 \gamma |\boldsymbol{s}|^{\gamma-1} (\ddot{\widetilde{\boldsymbol{x}}}_{\boldsymbol{2}} + \alpha_1 \dot{\widetilde{\boldsymbol{x}}}_{\boldsymbol{2}}) \tag{11}$$

substitute (10) into (11) yields

$$\dot{\sigma} = \dddot{\widetilde{\boldsymbol{x}}}_{\boldsymbol{2}} + \alpha_1 \ddot{\widetilde{\boldsymbol{x}}}_{\boldsymbol{2}} + \alpha_2 \gamma |\boldsymbol{s}|^{\gamma-1} (\ddot{\widetilde{\boldsymbol{x}}}_{\boldsymbol{2}} + \alpha_1 \dot{\widetilde{\boldsymbol{x}}}_{\boldsymbol{2}}) \tag{12}$$

by using (5), (13) can be achieved as

$$\begin{aligned} &\dot{\sigma} = \dot{F} + G\dot{\boldsymbol{u}} + \dot{G}\boldsymbol{u} + \alpha_1 (\ddot{\widetilde{\boldsymbol{x}}}_{\boldsymbol{2}} + \alpha_1 \dot{\widetilde{\boldsymbol{x}}}_{\boldsymbol{2}}) - \\ &\ddot{\boldsymbol{x}}_{\boldsymbol{2d}} + \alpha_2 \gamma |\boldsymbol{s}|^{\gamma-1} (\ddot{\widetilde{\boldsymbol{x}}}_{\boldsymbol{2}} + \alpha_1 \dot{\widetilde{\boldsymbol{x}}}_{\boldsymbol{2}}) = \\ &\dot{F} + G\dot{\boldsymbol{u}} + \dot{G}\boldsymbol{u} + (\alpha_1 + \alpha_2 \gamma |\boldsymbol{s}|^{\gamma-1}) (\ddot{\widetilde{\boldsymbol{x}}}_{\boldsymbol{2}} + \alpha_1 \dot{\widetilde{\boldsymbol{x}}}_{\boldsymbol{2}}) - \ddot{\boldsymbol{x}}_{\boldsymbol{2d}} \end{aligned} \tag{13}$$

with respect to (13), the derivative of the second sliding surface must be considered as zero. Since the derivative of the equivalent term of control signal is obtained as

$$\begin{aligned} \dot{\boldsymbol{u}}_{eq} = &- G^{-1} (\dot{F} + \dot{G}\boldsymbol{u} + (\alpha_1 + \alpha_2 \gamma |\boldsymbol{s}|^{\gamma-1}) \\ &(\ddot{\widetilde{\boldsymbol{x}}}_{\boldsymbol{2}} + \alpha_1 \dot{\widetilde{\boldsymbol{x}}}_{\boldsymbol{2}}) - \ddot{\boldsymbol{x}}_{\boldsymbol{2d}}) \end{aligned} \tag{14}$$

therefore, (15) demonstrates the equivalent term of the proposed control signal.

$$\begin{aligned} \boldsymbol{u}_{eq} = &- \int_0^T G^{-1} (\dot{F} + \dot{G}\boldsymbol{u} + (\alpha_1 + \alpha_2 \gamma |\boldsymbol{s}|^{\gamma-1}) \\ &(\ddot{\widetilde{\boldsymbol{x}}}_{\boldsymbol{2}} + \alpha_1 \dot{\widetilde{\boldsymbol{x}}}_{\boldsymbol{2}}) - \ddot{\boldsymbol{x}}_{\boldsymbol{2d}}) \end{aligned} \tag{15}$$

where T is the simulation time. Equation (1) presents the proposed exponential reaching term of the control signal.

$$\begin{aligned} \boldsymbol{u}_{sw} = &- \int_0^T G^{-1} \sum_{i=1}^{n} \boldsymbol{K}_{i1} sign(\boldsymbol{\sigma}_i) + \\ &\sum_{i=1}^{n} \boldsymbol{K}_{i2} |\boldsymbol{\sigma}_i|^{0.5} sign(\boldsymbol{\sigma}_i) + \\ &\sum_{i=1}^{n} (\boldsymbol{K}_{i3} |\boldsymbol{\sigma}_i| - 1) sign(\boldsymbol{\sigma}_i) dt \end{aligned} \tag{16}$$

https://dx.doi.org/10.57647/mjee.2026.2001.05

where n represents the number of control signals and is set to five.

Lemma 1: Considering, positive definite and a radially unbounded function V that satisfies the inequality $\dot{V}(x) + L_1 V(x) \leq 0$, where $L > 0$, it is shown that the tracking error of the robot system, as described in (1), converges to zero in finite time, thereby ensuring the closed-loop stability of the system.

Theorem 1: Consider the system (1), with respect to the assumptions (1)-(2) and the proposed control signal (17), Lemma 1 is fulfilled in a finite time.

$$\begin{aligned}\boldsymbol{u} = -\int_0^T G^{-1}(\dot{F} + \dot{G}\boldsymbol{u} + (\alpha_1 + \alpha_2\gamma|\boldsymbol{s}|^{\gamma-1}) \\ (\dot{\widetilde{\boldsymbol{x}}}_{\boldsymbol{2}} + \alpha_1\widetilde{\boldsymbol{x}}_{\boldsymbol{2}}) - \ddot{\boldsymbol{x}}_{\boldsymbol{2d}}) + \\ \sum_{i=1}^{n} \boldsymbol{K}_{i1} sign(\boldsymbol{\sigma}_{\boldsymbol{i}}) + \\ \sum_{i=1}^{n} \boldsymbol{K}_{i2}|\boldsymbol{\sigma}_{\boldsymbol{i}}|^{0.5} sign(\boldsymbol{\sigma}_{\boldsymbol{i}}) + \\ \sum_{i=1}^{n} (\boldsymbol{K}_{i3}{}^{|\boldsymbol{\sigma}_{\boldsymbol{i}}|} - 1) sign(\boldsymbol{\sigma}_{\boldsymbol{i}}) dt\end{aligned} \tag{17}$$

Proof.

Eqs. (18-19) expresses the Lyapunov candidate function and its derivative.

$$V_1 = \frac{1}{2}\boldsymbol{\sigma}^2 \tag{18}$$

$$\dot{V}_1 = \boldsymbol{\sigma}\dot{\boldsymbol{\sigma}} \tag{19}$$

Eq. (19) is turns into (20) based on (13) and (17).

$$\begin{aligned}&\dot{V}_1 = \boldsymbol{\sigma}(\dot{F} + G\dot{\boldsymbol{u}} + \dot{G}\boldsymbol{u} + (\alpha_1 + \alpha_2\gamma|\boldsymbol{s}|^{\gamma-1}) \\ &(\dot{\widetilde{\boldsymbol{x}}}_{\boldsymbol{2}} + \alpha_1\widetilde{\boldsymbol{x}}_{\boldsymbol{2}}) - \ddot{\boldsymbol{x}}_{\boldsymbol{2d}}) \\ &\dot{V}_1 = \boldsymbol{\sigma}(\dot{F} + G(G^{-1}(\dot{F} + \dot{G}\boldsymbol{u} + (\alpha_1 + \alpha_2\gamma|\boldsymbol{s}|^{\gamma-1}) \\ &(\dot{\widetilde{\boldsymbol{x}}}_{\boldsymbol{2}} + \alpha_1\widetilde{\boldsymbol{x}}_{\boldsymbol{2}}) - \ddot{\boldsymbol{x}}_{\boldsymbol{2d}}) + \sum_{i=1}^{n} \boldsymbol{K}_{i1} sign(\boldsymbol{\sigma}_{\boldsymbol{i}}) + \\ &\sum_{i=1}^{n} \boldsymbol{K}_{i2}|\boldsymbol{\sigma}_{\boldsymbol{i}}|^{0.5} sign(\boldsymbol{\sigma}_{\boldsymbol{i}}) + \\ &\sum_{i=1}^{n} (\boldsymbol{K}_{i3}{}^{|\boldsymbol{\sigma}_{\boldsymbol{i}}|} - 1) sign(\boldsymbol{\sigma}_{\boldsymbol{i}})) + \\ &\dot{G}\boldsymbol{u} + (\alpha_1 + \alpha_2\gamma|\boldsymbol{s}|^{\gamma-1})(\dot{\widetilde{\boldsymbol{x}}}_{\boldsymbol{2}} + \alpha_1\widetilde{\boldsymbol{x}}_{\boldsymbol{2}}) - \ddot{\boldsymbol{x}}_{\boldsymbol{2d}})\end{aligned} \tag{20}$$

with simplification of (20), yields

$$\dot{V}_1 = -\boldsymbol{\sigma}\left((\boldsymbol{K}_3{}^{|\boldsymbol{\sigma}|} - 1 + \boldsymbol{K}_1)\text{sign}(\boldsymbol{\sigma}) + \boldsymbol{K}_2|\boldsymbol{\sigma}|^{0.5}\text{sign}(\boldsymbol{\sigma})\right) \tag{21}$$

Eq. (21) is divided into two parts as follows.

$$\dot{V}_{1-1} = \left((\boldsymbol{K}_3{}^{|\boldsymbol{\sigma}|} - 1) + \boldsymbol{K}_1\right)|\boldsymbol{\sigma}| \geq 0 \tag{22}$$

$$\dot{V}_{1-2} = \boldsymbol{K}_2|\boldsymbol{\sigma}|^{1.5} \geq 0 \tag{23}$$

Both of these terms are semi-positive definite, which implies that their sum must also be semi-positive definite. Consequently, we have:

$$\dot{V}_1 \leq 0 \tag{24}$$

According to LaSalle's Invariant Set Theorem, when $\boldsymbol{\sigma} = 0$, the derivative of the Lyapunov function $\dot{V}_1$ vanishes, indicating that the system will reach a state where $\boldsymbol{\sigma} = 0$. At this point, the state tracking error will converge to zero, which ensures global finite-time stability. Therefore, it is guaranteed that the system's tracking error asymptotically approaches zero as time progresses.

Q.E.D.

2.3 ELM

ELM is a type of single-hidden layer feedforward neural network that relies on randomly generated initial values for its parameters. Specifically, the weights and biases of the hidden layer are randomly initialized without any prior knowledge, and remain constant throughout the training and testing process. In contrast, the output layer parameters, including the weights and biases, are trained using gradient descent or other optimization algorithms, allowing the model to learn and adapt to the data. This unique approach enables ELM to achieve fast and efficient training, making it a popular choice for a wide range of applications [29]. This paper employs a direct adaptive approach to estimate the optimal values of the controller parameters. The ELM contains three vectors of the system states, tracking errors, and secondary sliding surface $(\boldsymbol{x}, \widetilde{\boldsymbol{x}}, \boldsymbol{\sigma})$ and two vectors of the controller parameters $(\widehat{K}_1, \widehat{K}_2)$. The estimated parameters using the proposed ELM is represented as

$$\begin{aligned}&\widehat{\boldsymbol{K}}_1(\boldsymbol{x}, \widetilde{\boldsymbol{x}}, \boldsymbol{\sigma}|\widehat{W}_1, \widehat{B}_1) = \\ &\widehat{W}_1^T(\boldsymbol{H}(\boldsymbol{x}, \widetilde{\boldsymbol{x}}, \boldsymbol{\sigma})) + \widehat{B}_1 = \widehat{W}_1^T(\boldsymbol{H}) + \widehat{B}_1\end{aligned} \tag{25}$$

$$\begin{aligned}&\widehat{\boldsymbol{K}}_2(\boldsymbol{x}, \widetilde{\boldsymbol{x}}, \boldsymbol{\sigma}|\widehat{W}_2, \widehat{B}_2) = \\ &\widehat{W}_2^T(\boldsymbol{H}(\boldsymbol{x}, \widetilde{\boldsymbol{x}}, \boldsymbol{\sigma})) + \widehat{B}_2 = \widehat{W}_2^T(\boldsymbol{H}) + \widehat{B}_2\end{aligned} \tag{26}$$

Here, $\widehat{W}_1$, and $\widehat{W}_2$ represent the estimated weights, $\widehat{B}_1$, and $\widehat{B}_2$ are the estimated biases of the output layer weights $\widehat{K}_1$, $\widehat{K}_2$ respectively, while w, and b denote the weights and biases of the hidden layer. The optimal parameter of W_F^* and B_F^* can be defined as follows.

$$(W_1^*, B_1^*) = \arg\min[\sup|\boldsymbol{K}_1^* - \widehat{\boldsymbol{K}}_1(\boldsymbol{x}, \widetilde{\boldsymbol{x}}, \boldsymbol{\sigma}|\widehat{W}_1, \widehat{B}_1)|] \tag{27}$$

$$(W_2^*, B_2^*) = \arg\min[\sup|\boldsymbol{K}_2^* - \widehat{\boldsymbol{K}}_2(\boldsymbol{x}, \widetilde{\boldsymbol{x}}, \boldsymbol{\sigma}|\widehat{W}_2, \widehat{B}_2)|] \tag{28}$$

where W_1^*, and W_2^* denote the optimal weights, B_1^*, and B_2^* are the optimal biases of $\widehat{\boldsymbol{K}}_1$, $\widehat{\boldsymbol{K}}_2$, respectively. As a result, the error estimates of the optimal parameters are defined as

$$\widetilde{W}_1 = W_1^* - \widehat{W}_1, \ \widetilde{B}_1 = B_1^* - \widehat{B}_1 \tag{29}$$

$$\widetilde{W}_2 = W_2^* - \widehat{W}_2, \ \widetilde{B}_2 = B_2^* - \widehat{B}_2 \tag{30}$$

According to (27)-(30), the estimation error of $\widehat{\boldsymbol{K}}_1$, $\widehat{\boldsymbol{K}}_2$ are presented in (31)-(32).

$$\begin{aligned}&\widetilde{\boldsymbol{K}}_1(\boldsymbol{x}, \widetilde{\boldsymbol{x}}, \boldsymbol{\sigma}|\widetilde{W}_1, \widetilde{B}_1) = \\ &\boldsymbol{K}_1^* - \widehat{\boldsymbol{K}}_1(\boldsymbol{x}, \widetilde{\boldsymbol{x}}, \boldsymbol{\sigma}|\widehat{W}_1, \widehat{B}_1) = \widehat{W}_1^T(\boldsymbol{H}) + \widetilde{B}_1\end{aligned} \tag{31}$$

https://dx.doi.org/10.57647/mjee.2026.2001.05

$$\widetilde{\boldsymbol{K}}_2(\boldsymbol{x},\widetilde{\boldsymbol{x}},\boldsymbol{\sigma}|\widetilde{W}_2,\widetilde{B}_2) = \boldsymbol{K}_2^* - \widehat{\boldsymbol{K}}_2(\boldsymbol{x},\widetilde{\boldsymbol{x}},\boldsymbol{\sigma}|\widehat{W}_2,\widehat{B}_2) = \widehat{W}_2^T(\boldsymbol{H}) + \widetilde{B}_2 \tag{32}$$

The initial values of the tunable parameters in ELMs can be randomly selected, and the output weights and biases are adaptively adjusted using adaptive control laws derived from the Lyapunov candidate function.

2.4 Stability analysis of ADTSMC using ELM

This subsection investigates the Lyapunov stability of the proposed ADTSMC integrated with the ELM, employing Theorem 2 for the stability analysis.

Theorem 2: Considering the 5-DOF upper-limb exoskeleton robot system and the assumptions (1-2), Lemma 2 is satisfied, if the control signal is expressed as

$$\boldsymbol{u} = -\int_0^T G^{-1}(\dot{F} + \dot{G}\boldsymbol{u} + (\alpha_1 + \alpha_2\gamma|\boldsymbol{s}|^{\gamma-1}) (\dot{\widetilde{\boldsymbol{x}}}_2 + \alpha_1\widetilde{\boldsymbol{x}}_2) - \ddot{\boldsymbol{x}}_{2d}) + \widehat{\boldsymbol{K}}_1 sign(\boldsymbol{\sigma}) + \widehat{\boldsymbol{K}}_2|\boldsymbol{\sigma}|^{0.5}sign(\boldsymbol{\sigma}) + (\boldsymbol{K}_3{}^{|\boldsymbol{\sigma}|} - 1)dt \tag{33}$$

with the adaptation control laws as (34)-(37)

$$\dot{\widehat{W}}_1 = -\frac{\eta}{2}|\boldsymbol{\sigma}|(\boldsymbol{H}) \tag{34}$$

$$\dot{\widehat{B}}_1 = -\frac{\eta}{2}|\boldsymbol{\sigma}| \tag{35}$$

$$\dot{\widehat{W}}_2 = -\frac{\eta}{2}|\boldsymbol{\sigma}|^{1.5}(\boldsymbol{H}) \tag{36}$$

$$\dot{\widehat{B}}_2 = -\frac{\eta}{2}|\boldsymbol{\sigma}|^{1.5} \tag{37}$$

Proof. A Lyapunov candidate function is proposed as given in equation (38).

$$V_2 = \frac{1}{2}\boldsymbol{\sigma}^2 + \frac{1}{\eta}\sum_{j=1}^{n}\sum_{i=1}^{p}\widetilde{W}_{ij1}^T\widetilde{W}_{ij1} + \frac{1}{\eta}\sum_{j=1}^{n}\sum_{i=1}^{p}\widetilde{W}_{ij2}^T\widetilde{W}_{ij2} + \frac{1}{\eta}\sum_{i=1}^{2}\widetilde{B}_i\widetilde{B}_i \tag{38}$$

Eq. (39) gives the derivative of the Lyapunov candidate function

$$\dot{V}_2 = \boldsymbol{\sigma}\dot{\boldsymbol{\sigma}} - \frac{2}{\eta}\sum_{j=1}^{n}\sum_{i=1}^{p}\widetilde{W}_{ij1}^T\dot{\widehat{W}}_{ij1} - \frac{2}{\eta}\sum_{j=1}^{n}\sum_{i=1}^{p}\widetilde{W}_{ij2}^T\dot{\widehat{W}}_{ij2} - \frac{2}{\eta}\sum_{i=1}^{2}\widetilde{B}_i^T\dot{\widehat{B}}_i \tag{39}$$

With replacing (32) into (39), (40) is achieved as follows

$$\dot{V}_2 = \boldsymbol{\sigma}\left(((K_3{}^{|\boldsymbol{\sigma}|} - 1) + \widehat{K}_1)sign(\boldsymbol{\sigma}) + (\widehat{K}_2)|\boldsymbol{\sigma}|^{0.5}sign(\boldsymbol{\sigma})\right) - \frac{2}{\eta}\sum_{j=1}^{n}\sum_{i=1}^{p}\widetilde{W}_{ij1}^T\dot{\widehat{W}}_{ij1} - \frac{2}{\eta}\sum_{j=1}^{n}\sum_{i=1}^{p}\widetilde{W}_{ij2}^T\dot{\widehat{W}}_{ij2} - \frac{2}{\eta}\sum_{i=1}^{2}\widetilde{B}_i^T\dot{\widehat{B}}_i \tag{40}$$

By substituting the optimal values of the controller parameters, (40) turns into (41).

$$\dot{V}_2 = \boldsymbol{\sigma}\Big(((K_3{}^{|\boldsymbol{\sigma}|} - 1) + \widehat{W}_1^T(\boldsymbol{H}) + \widehat{B}_1)sign(\boldsymbol{\sigma}) + (\widehat{W}_2^T(\boldsymbol{H}) + \widehat{B}_2)|\boldsymbol{\sigma}|^{0.5}sign(\boldsymbol{\sigma})\Big) - \frac{2}{\eta}\sum_{j=1}^{n}\sum_{i=1}^{p}\widetilde{W}_{ij1}^T\dot{\widehat{W}}_{ij1} - \frac{2}{\eta}\sum_{j=1}^{n}\sum_{i=1}^{p}\widetilde{W}_{ij2}^T\dot{\widehat{W}}_{ij2} - \frac{2}{\eta}\sum_{i=1}^{2}\widetilde{B}_i^T\dot{\widehat{B}}_i \tag{41}$$

$$\dot{V}_2 = -\boldsymbol{\sigma}\Bigg(\Big((K_3{}^{|\boldsymbol{\sigma}|} - 1) + \underbrace{\widehat{W}_1^T(\boldsymbol{H}) - \widehat{W}_1^{*T}(\boldsymbol{H})}_{=-\widetilde{W}_1^T(\boldsymbol{H})} + \widehat{W}_1^{*T}(\boldsymbol{H}) + \underbrace{\widehat{B}_1 - \widehat{B}_1^*}_{=-\widetilde{B}_1} + \widehat{B}_1^*\Big)sign(\boldsymbol{\sigma}) + \Big(\underbrace{\widehat{W}_2^T(\boldsymbol{H}) - \widehat{W}_2^{*T}(\boldsymbol{H})}_{=-\widetilde{W}_2^T(\boldsymbol{H})} + \widehat{W}_2^{*T}(\boldsymbol{H}) + \underbrace{\widehat{B}_2 - \widehat{B}_2^*}_{=-\widetilde{B}_2} + \widehat{B}_2^*\Big)|\boldsymbol{\sigma}|^{0.5}sign(\boldsymbol{\sigma})\Bigg) - \frac{2}{\eta}\sum_{j=1}^{n}\sum_{i=1}^{p}\widetilde{W}_{ij1}^T\dot{\widehat{W}}_{ij1} - \frac{2}{\eta}\sum_{j=1}^{n}\sum_{i=1}^{p}\widetilde{W}_{ij2}^T\dot{\widehat{W}}_{ij2} - \frac{2}{\eta}\sum_{i=1}^{2}\widetilde{B}_i^T\dot{\widehat{B}}_i \tag{42}$$

(42) is divided into three parts as

$$\dot{V}_{2-1} = \boldsymbol{\sigma}(\widetilde{W}_1^T(\boldsymbol{H}) + \widetilde{B}_1 + \widehat{W}_1^{*T}(\boldsymbol{H}) + B_1^*)sign(\boldsymbol{\sigma}) - \frac{2}{\eta}\sum_{j=1}^{n}\sum_{i=1}^{p}\widetilde{W}_{ij1}^T\dot{\widehat{W}}_{ij1} - \frac{2}{\eta}\widetilde{B}_1\dot{\widehat{B}}_1 \tag{43}$$

$$\dot{V}_{2-2} = \boldsymbol{\sigma}(\widetilde{W}_2^T(\boldsymbol{H}) + \widetilde{B}_2 + \widehat{W}_2^{*T}(\boldsymbol{H}) + B_2^*)|\boldsymbol{\sigma}|^{0.5} sign(\boldsymbol{\sigma}) - \frac{2}{\eta}\sum_{j=1}^{n}\sum_{i=1}^{p}\widetilde{W}_{ij2}^T\dot{\widehat{W}}_{ij2} - \frac{2}{\eta}\widetilde{B}_2\dot{\widehat{B}}_2 \tag{44}$$

$$\dot{V}_{2-3} = \boldsymbol{\sigma}(\boldsymbol{K}_3{}^{|\boldsymbol{\sigma}|} - 1)sign(\boldsymbol{\sigma}) \tag{45}$$

The estimation error i.e., $\widehat{W}_1$, $\widehat{B}_1$, $\widehat{W}_2$, and $\widehat{B}_2$ converge to zero using (34)-(37); and thus (43)-(45) can be expressed as

$$\dot{V}_{2-1} = -\boldsymbol{\sigma}(W_1^{*T}(\boldsymbol{H}) + B_1^*)sign(\boldsymbol{\sigma}) = (W_1^{*T}(\boldsymbol{H}) + B_1^*)|\boldsymbol{\sigma}| \tag{46}$$

$$\dot{V}_{2-2} = -\boldsymbol{\sigma}(W_2^{*T}(\boldsymbol{H}) + B_2^*)|\boldsymbol{\sigma}|^{0.5}sign(\boldsymbol{\sigma}) = (W_2^{*T}(\boldsymbol{H}) + B_2^*)|\boldsymbol{\sigma}|^{1.5} \tag{47}$$

$$\dot{V}_{2-3} = -\boldsymbol{\sigma}(\boldsymbol{K}_3{}^{|\boldsymbol{\sigma}|} - 1)sign(\boldsymbol{\sigma}) = (\boldsymbol{K}_3{}^{|\boldsymbol{\sigma}|} - 1)|\boldsymbol{\sigma}| \tag{48}$$

According to (46)-(48), the three parts of $\dot{V}_2$ are the non-positive part; hence the time derivative of the Lyapunov candidate function can be expressed in (49).

https://dx.doi.org/10.57647/mjee.2026.2001.05

$$\dot{V}_2 = \dot{V}_{2-1} + \dot{V}_{2-2} + \dot{V}_{2-3} \leq 0 \tag{49}$$

As per the LaSalle Invariant Set Theorem, the set of states for which $\dot{V}_2$ will be the largest invariant set where $\boldsymbol{\sigma} = 0$, which indicates that the tracking error $\boldsymbol{\sigma}$ will asymptotically converge to zero. Hence, the system's state will eventually enter the region where $\dot{V}_2$, which corresponds to $\boldsymbol{\sigma} = 0$.

Furthermore, applying Barbalat's Lemma, we know that if the time derivative of a Lyapunov function is negative semi-definite and the Lyapunov function is bounded, then the state converges to zero asymptotically. Since $\dot{V}_2 \leq 0$ and $\dot{V}_2$ is bounded, this ensures that the tracking error $\boldsymbol{\sigma}$ converges to zero in finite time. Therefore, the closed-loop stability of the system is guaranteed, and the proof is complete.

Q.E.D.

Figure 2 depicts the block diagram of the proposed ADTSMC with an exponential term and the ELM for the position control of the robot.

The ADTSMC with ELM, while offering robust performance, may encounter challenges with computational complexity, particularly in systems with high degrees of freedom or dynamic environments, which could slow real-time adaptation. Additionally, the performance of the ELM network is sensitive to initial conditions and requires careful tuning for optimal results. Lastly, when scaling to larger systems or implementing in real-time applications with limited computational resources, there may be a need to balance performance with computational efficiency to ensure effective operation.

The initial parameters are set as follows: $\alpha_1 = 1.5$, $\alpha_2 = 0.75$, $\gamma = 1.3$, $K_1 = 9.5$, $K_2 = 7.1$, and $K_3 = 1.25$. The ELM has one layer with 10 neurons. These parameters were obtained through a trial-and-error process, where different values were tested to balance convergence, stability, and robustness, ensuring the system adapts effectively to uncertainties and disturbances.

3. Results and discussion

This section presents the evaluation of the proposed control approach through two distinct scenarios, aiming to demonstrate its generality, robustness, and superiority. The performance of various control methods, including SMC, DSMC, DSMC with exponential term, DTSMC with exponential term, and ADTSMC with exponential term, is compared. Additionally, the performance of the adaptive SMC with fuzzy neural network proposed in [27] is assessed to verify the effectiveness of the presented ADTSMC with exponential term. To facilitate a comprehensive evaluation and comparison, statistical analysis is employed, including Integral Square Error (ISE), Integral Time Square Error (ITSE), Average Chattering Magnitude (ACM), and Control Energy (CE). The formulas for these performance indices are provided in equations (50)-(53).

$$\text{ISE} = \int_0^T \tilde{\boldsymbol{x}}^T \tilde{\boldsymbol{x}} dt \tag{50}$$

$$\text{ISE} = \int_0^T t.\tilde{\boldsymbol{x}}^T \tilde{\boldsymbol{x}} dt \tag{51}$$

$$\text{ACM} = \text{RMS}(\sqrt{\tilde{\boldsymbol{x}}^T \tilde{\boldsymbol{x}}} - \sqrt{\boldsymbol{x_d}^T \boldsymbol{x_d}}) \tag{52}$$

$$\text{CE} = \int_0^T (u^T u) dt \tag{53}$$

It's worth noting that in the context of these performance metrics, lower values are generally preferred. For example, a smaller CE value indicates more efficient control efforts, while lower values for ISE, ITSE, and ACM suggest improved trajectory tracking and reduced chattering effects. The 5-DOF upper-limb exoskeleton robot system models, along with the various controllers, are implemented and simulated using the MATLAB/SIMULINK environment.

3.1 First scenario

In this scenario, the desired trajectory is supposed as

$$\boldsymbol{x_d}(0) = [\sin(t + \frac{\pi}{5}), \sin(t + \frac{2\pi}{5}), \sin(t + \frac{3\pi}{5}), \sin(t + \frac{4\pi}{5}), \sin(t + \frac{6\pi}{5})].$$

The initial states are set to zero, and the system is not affected by external disturbances. To enhance the clarity and readability of the figures, we have chosen to display the state trajectories for x_3 and x_5, along with the control signals u_3 and u_5. This focused presentation aims to improve visual coherence and facilitate a clearer

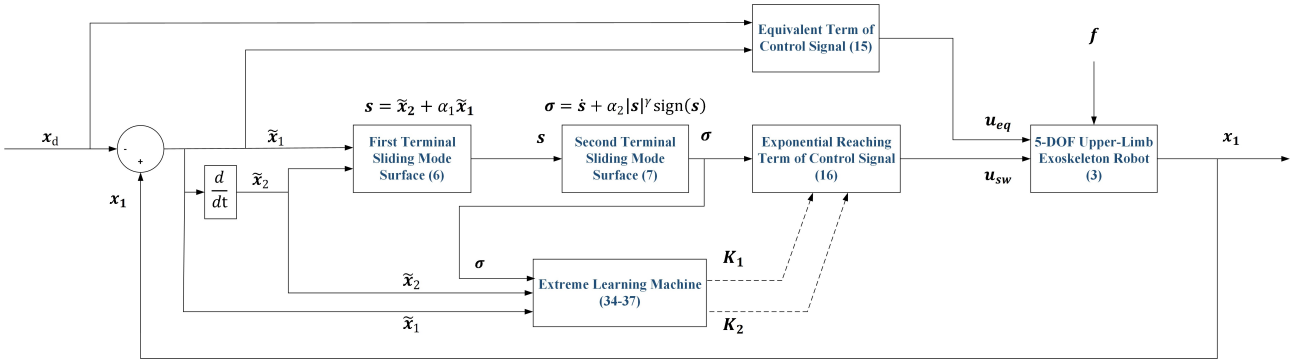

Figure 2. Block diagram of the ADTSMC with exponential term for position control of the robot.

https://dx.doi.org/10.57647/mjee.2026.2001.05

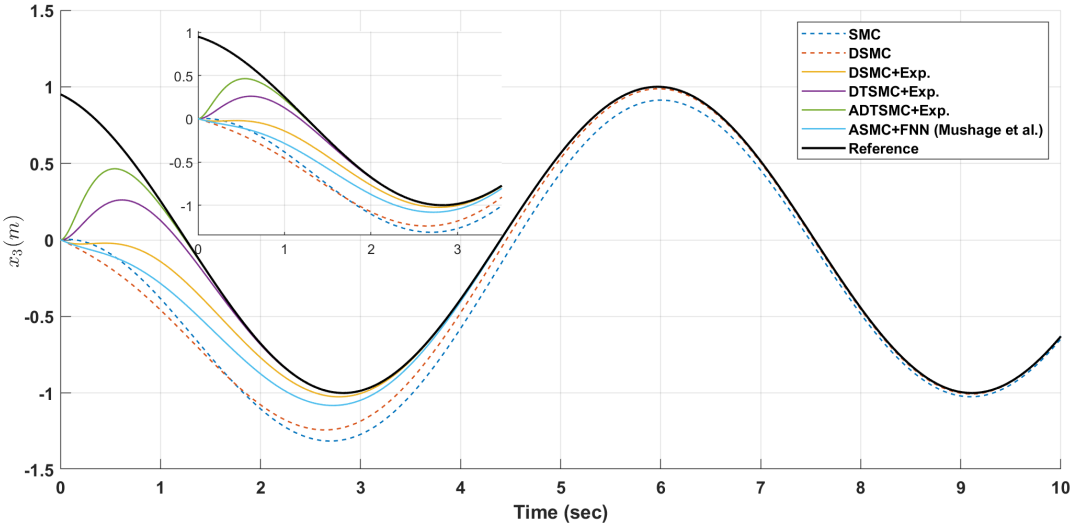

Figure 3. The trajectory of x_3 using the SMC, DSMC, DSMC with exponential term, DTSMC with exponential term, ADTSMC with exponential term, and ASMC with FNN [27] in the first example.

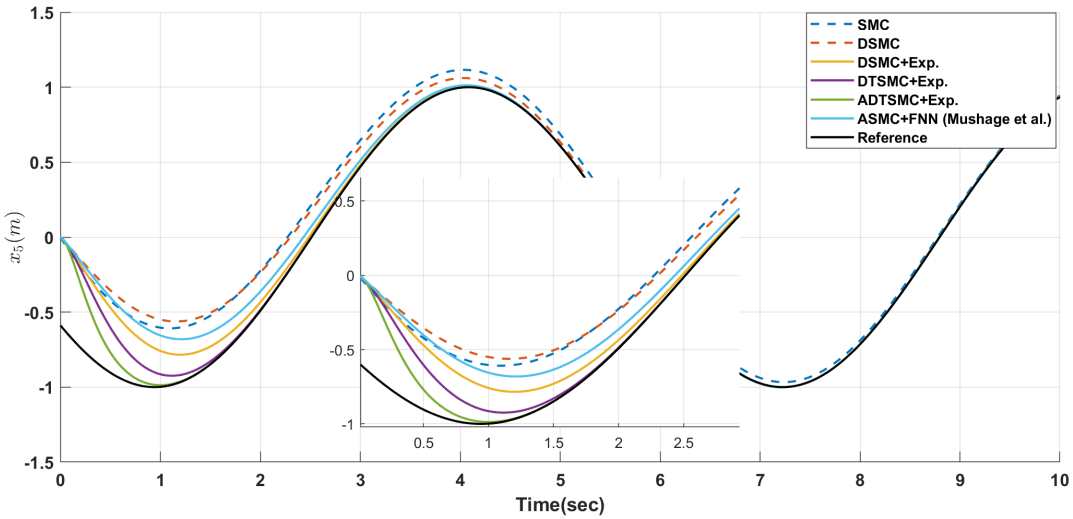

Figure 4. The trajectory of x_5 using the SMC, DSMC, DSMC with exponential term, DTSMC with exponential term, ADTSMC with exponential term, and ASMC with FNN [27] in the first example.

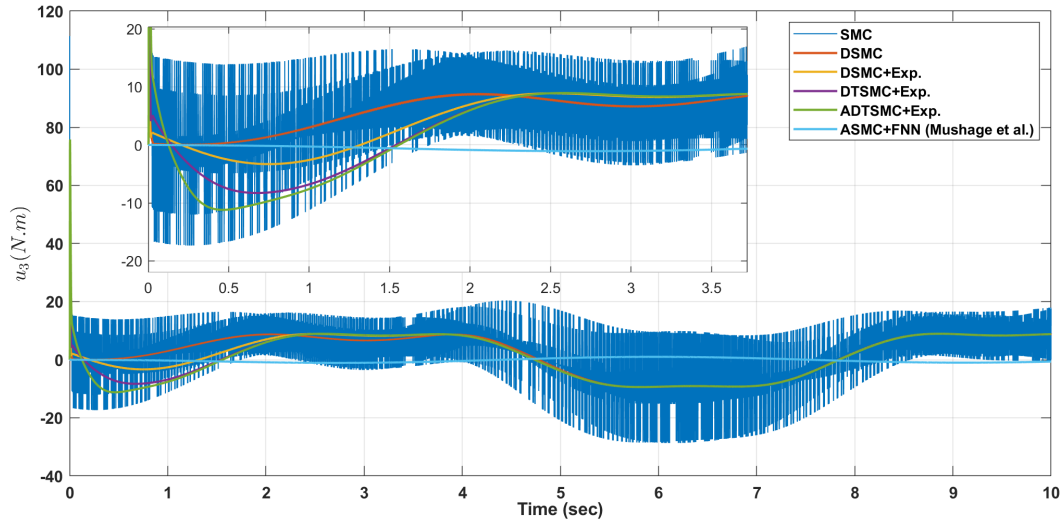

Figure 5. The third control signal (u_3) using the SMC, DSMC, DSMC with exponential term, DTSMC with exponential term, ADTSMC with exponential term, and ASMC with FNN [27] in the first example.

https://dx.doi.org/10.57647/mjee.2026.2001.05

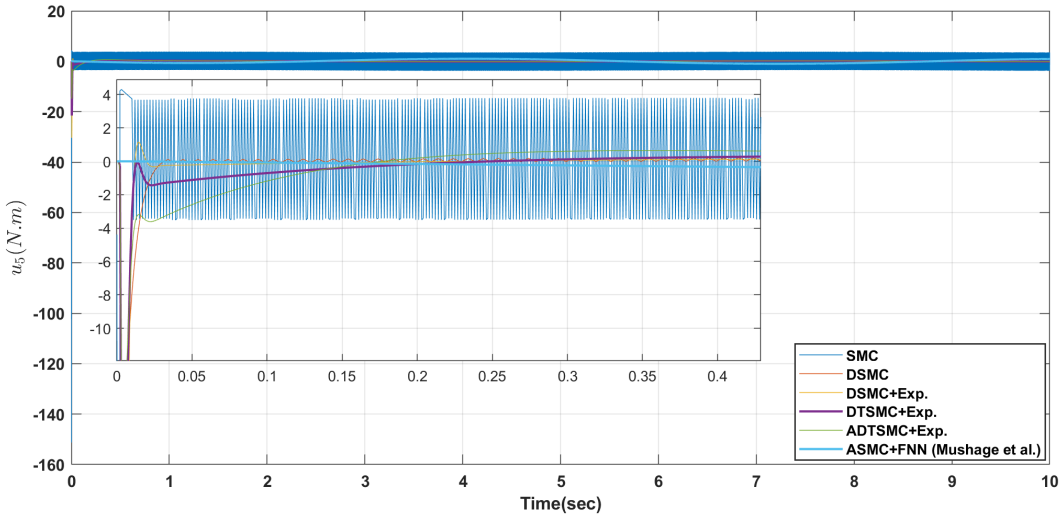

Figure 6. The fifth control signal (u_5) using the SMC, DSMC, DSMC with exponential term, DTSMC with exponential term, ADTSMC with exponential term, and ASMC with FNN [27] in the first example.

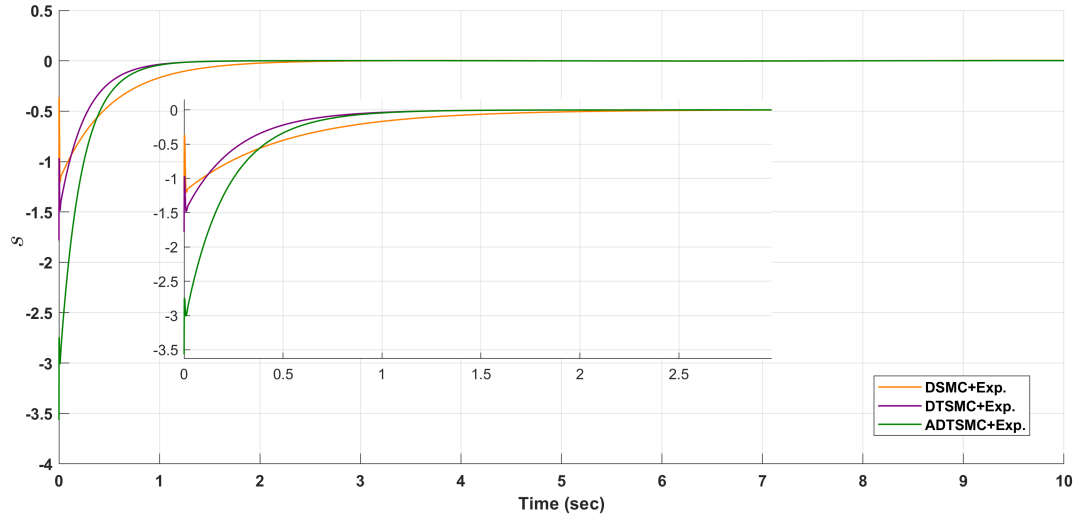

Figure 7. The first sliding surface (s) in the DSMC with exponential term, DTSMC with exponential term, and ADTSMC with exponential term in the first example.

interpretation of the results. The results of the first scenario are presented in figures 3- 9 and Table 1.

Figures 7 and 8 show the profile of the sliding surfaces over time in the first example.

According to Figures 7- 8, defined in equations (6) and (7), demonstrate their convergence and boundedness, which are crucial for assessing the control performance of DSMC, DTSMC, and ADTSMC. The sliding surface $\boldsymbol{s}$ converges to zero over time, indicating effective error reduction, with DTSMC and ADTSMC achieving faster convergence and better dynamic adaptation compared to DSMC. The boundedness of ss is evident, with minimal overshoots and oscillations, ensuring stability. Similarly, $\boldsymbol{\sigma}$ shows smooth convergence to zero, reflecting stabilization of the sliding surface dynamics. DTSMC displays a less aggressive decay with reduced oscillations, while ADTSMC further enhances robustness against disturbances. Overall, the plots validate the superior performance of DTSMC and ADTSMC in terms of faster convergence, smoother behavior, and robust boundedness of $\boldsymbol{s}$ and $\boldsymbol{\sigma}$ compared to DSMC.

Figure 9 illustrates the adaptive control gains in ADTSMC with an exponential term in the first example.

Based on the Fig. 9, these gains of $\widehat{K}_1$ and $\widehat{K}_2$ adjust dynamically to system uncertainties and disturbances, ensuring stability and performance by modulating the control effort based on system requirements. Smooth transitions in the gain profiles suggest robustness, preventing instability and excessive oscillations. The adaptive control laws govern the real-time updates of the parameters $\widehat{W}_1$, $\widehat{W}_2$, $\widehat{B}_1$, and $\widehat{B}_2$, which are influenced by the system's state and sliding surface information. The laws slow adaptation when the error approaches zero, preventing abrupt changes near equilibrium, and accelerate convergence during high-error conditions, ensuring precise control as the error diminishes. These dynamic adjustments enhance the system's robustness and effectiveness, particularly in real-world applications

https://dx.doi.org/10.57647/mjee.2026.2001.05

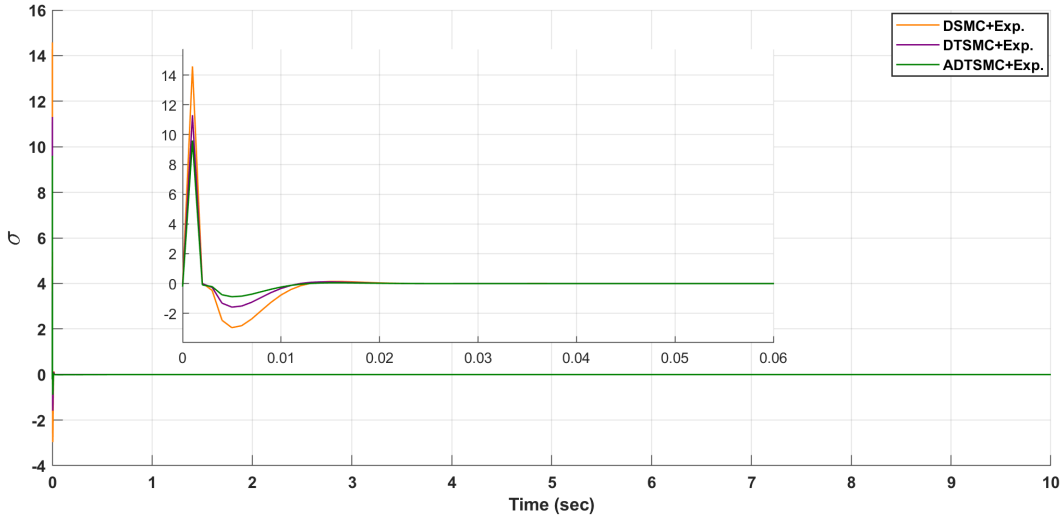

Figure 8. The second sliding surface (σ) in the DSMC with exponential term, DTSMC with exponential term, and ADTSMC with exponential term in the first example.

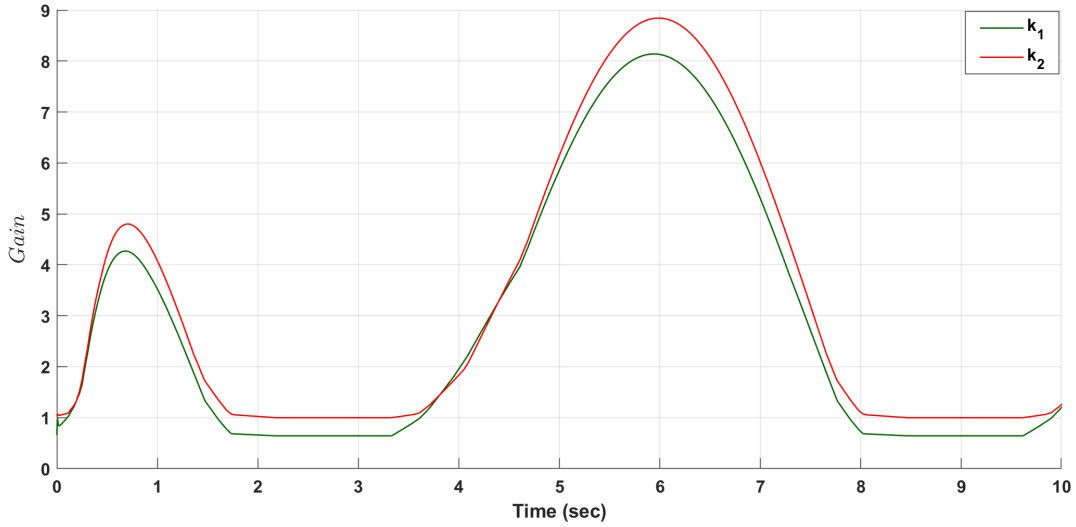

Figure 9. The adaptive control gains in ADTSMC with exponential term in the first example.

such as robotics, where the system must adapt to unpredictable environments. The adaptive gains ensure stability and performance by enabling the system to respond to varying conditions while minimizing control effort.

3.2 Second scenario

In this scenario, the desired trajectory is supposed as

$$\boldsymbol{x_d}(0) = 3 * [\sin(0.8t + \frac{\pi}{5}), \sin(0.8t + \frac{2\pi}{5}), \sin(0.8t + \frac{3\pi}{5}), \sin(0.8t + \frac{4\pi}{5}), \sin(0.8t + \frac{6\pi}{5})].$$

Table 1. Control results in the first example using the SMC, DSMC, DSMC with exponential term, DTSMC with exponential term, ADTSMC with exponential term, and ASMC with FNN [27].

Controller	ISE (m^2)	ITSE (m^2sec)	CE ((N·m)^{2}sec)	ACMn (m)
SMC	3.6057	4.4902	328947.46	9.7446×10^{-2}
DSMC	3.6318	3.3252	11887.85	7.1734×10^{-3}
DSMC with exponential term	1.7971	0.8160	9324.22	5.1365×10^{-3}
DTSMC with exponential term	0.9736	0.2467	6364.05	4.6420×10^{-3}
ADTSMC with exponential term	0.6231	0.1053	5336.67	4.0559×10^{-3}
ASMC with FNN [27]	2.4258	1.4845	12505.46	9.1431×10^{-3}

https://dx.doi.org/10.57647/mjee.2026.2001.05

The initial states are considered as

$$\boldsymbol{x}(0) = [0.8, 0.8, -2, -2, 0.2]$$

$$\dot{\boldsymbol{x}}(0) = [-0.8, -0.8, 2, 2, -0.2]$$

and the external disturbance is presented as

$$f(t) = 5 * [\sin(3t), \sin(3t + \frac{2\pi}{5}), \sin(3t + \frac{3\pi}{5}), \sin(3t + \frac{4\pi}{5}), \sin(3t + \frac{6\pi}{5})] * u(t-5).$$

where $u(t)$ is the step function. Disturbances in the system primarily arise from the forces applied by the user and the intricate interactions between the human operator and the robot. These inherent disturbances, stemming from the dynamic nature of human-robot interaction, highlight the indispensable need for employing a sophisticated controller to ensure effective trajectory tracking. In the second scenario, the length of the arm is increased by 20% to introduce parametric uncertainty. Additionally, a trajectory error plot is included to provide a more comprehensive comparison. The performance of the controllers in this scenario is presented in figures 10- 18 and Table 2.

The sliding surfaces are illustrated over time in figures 16 and 17.

Equations (18) and (19) demonstrate the convergence and boundedness of the sliding surface ss, which are key for assessing the control performance of DSMC, DTSMC, and ADTSMC. Over time, ss converges to zero, showing effective error reduction, with DTSMC and ADTSMC achieving faster convergence and better dynamic adaptation than DSMC. The boundedness of ss is maintained, ensuring stability, and $\boldsymbol{\sigma}$ smoothly converges to zero, reflecting stabilization. DTSMC shows a less aggressive decay with fewer oscillations, while ADTSMC outperforms all, offering the fastest convergence, smoothest behavior, and best robustness against disturbances. Overall, ADTSMC demonstrates superior performance compared to DSMC and DTSMC.

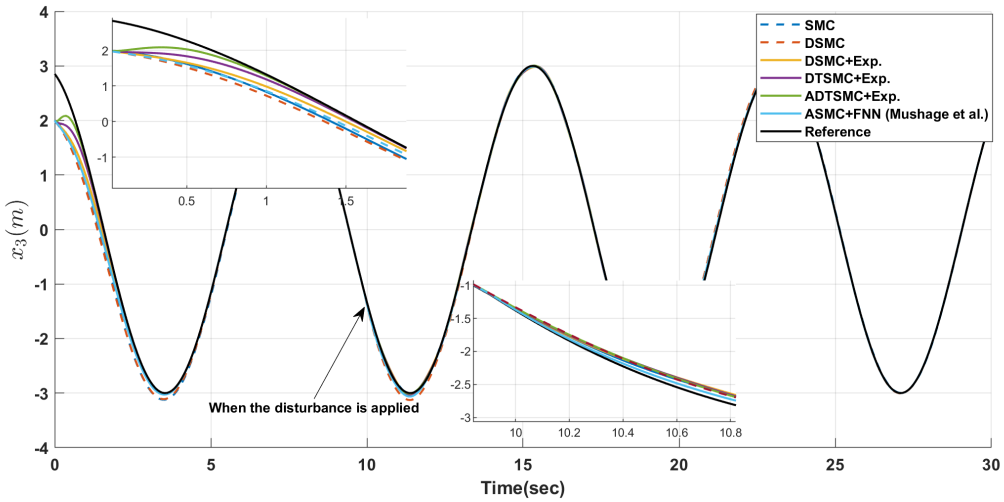

Figure 10. The trajectory of x_3 using the SMC, DSMC, DSMC with exponential term, DTSMC with exponential term, ADTSMC with exponential term, and ASMC with FNN [27] in the second example.

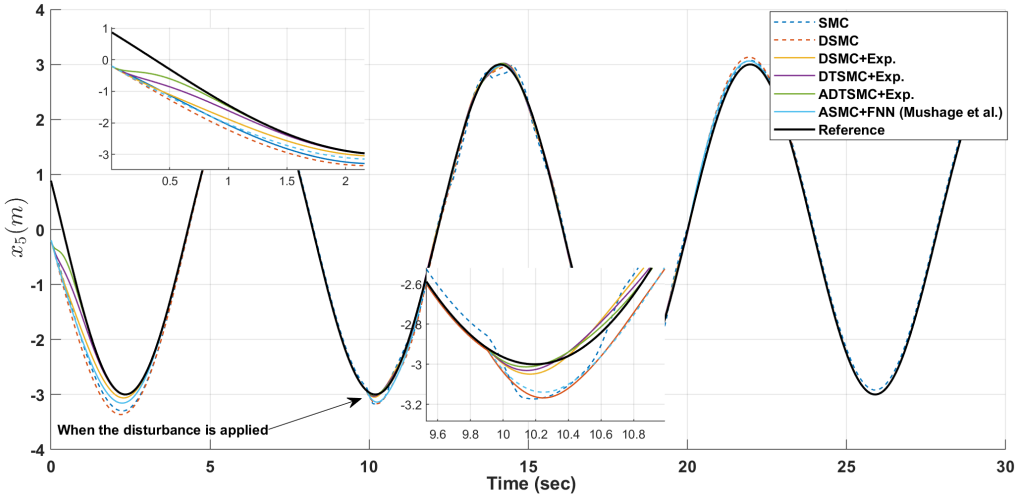

Figure 11. The trajectory of x_5 using the SMC, DSMC, DSMC with exponential term, DTSMC with exponential term, ADTSMC with exponential term, and ASMC with FNN [27] in the second example.

https://dx.doi.org/10.57647/mjee.2026.2001.05

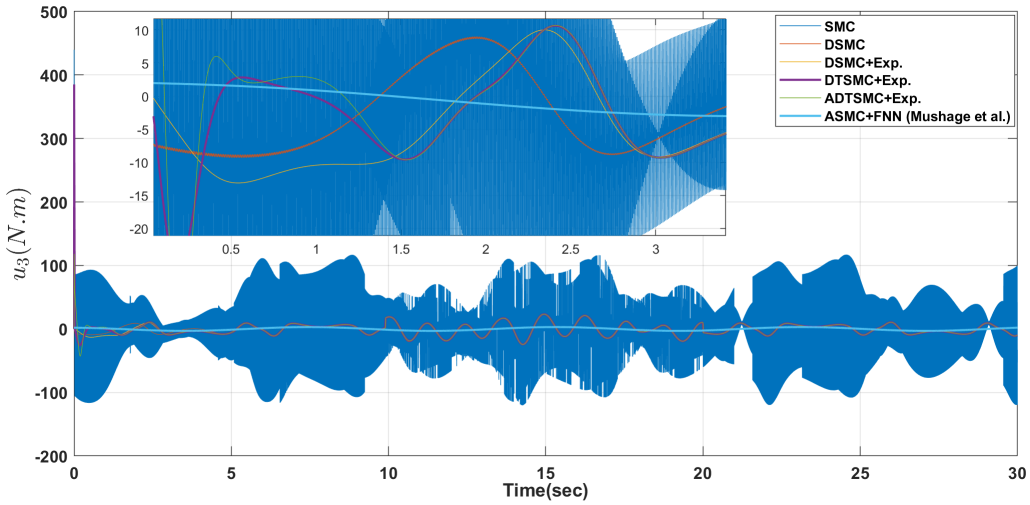

Figure 12. The third control signal (u_3) using the SMC, DSMC, DSMC with exponential term, DTSMC with exponential term, ADTSMC with exponential term, and ASMC with FNN [27] in the second example.

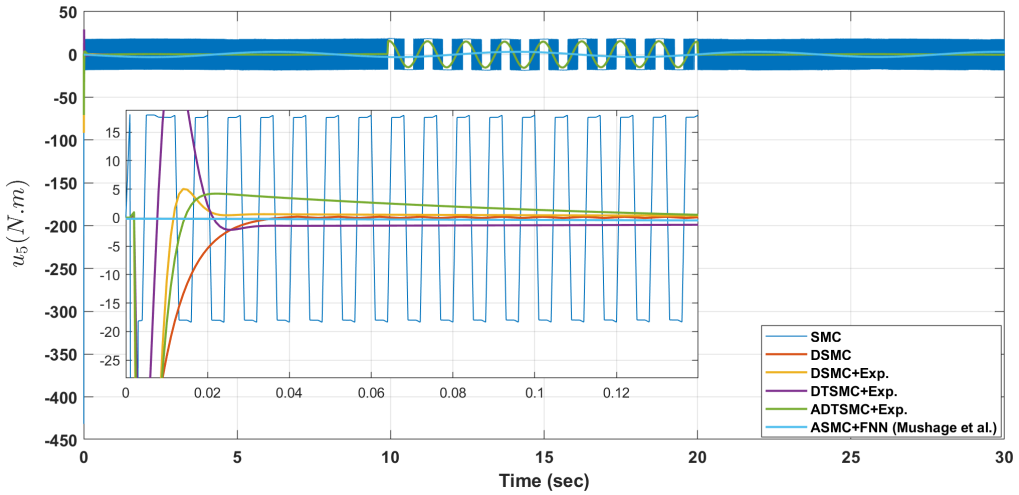

Figure 13. The fifth control signal (u_5) using the SMC, DSMC, DSMC with exponential term, DTSMC with exponential term, ADTSMC with exponential term, and ASMC with FNN [27] in the second example.

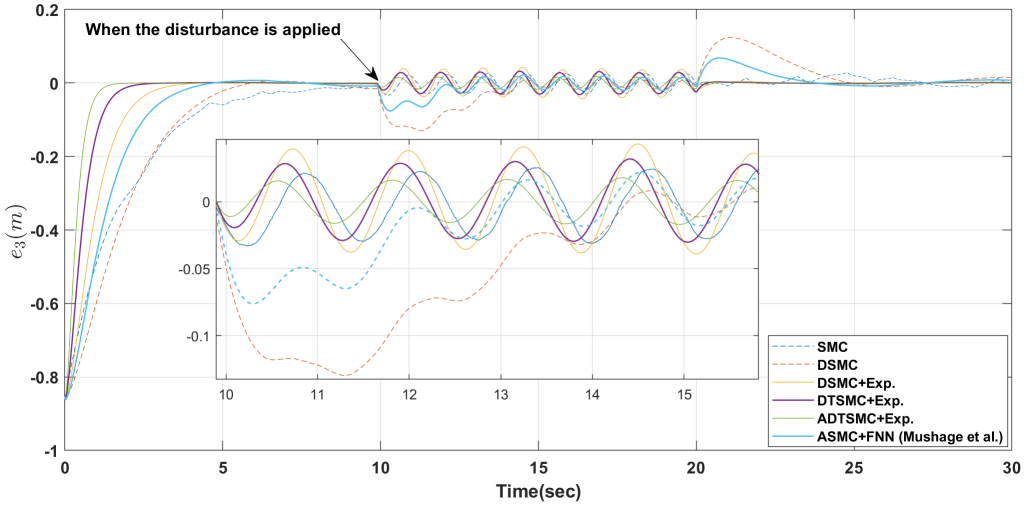

Figure 14. The error trajectory of e_3 using the SMC, DSMC, DSMC with exponential term, DTSMC with exponential term, ADTSMC with exponential term, and ASMC with FNN [27] in the second example.

https://dx.doi.org/10.57647/mjee.2026.2001.05

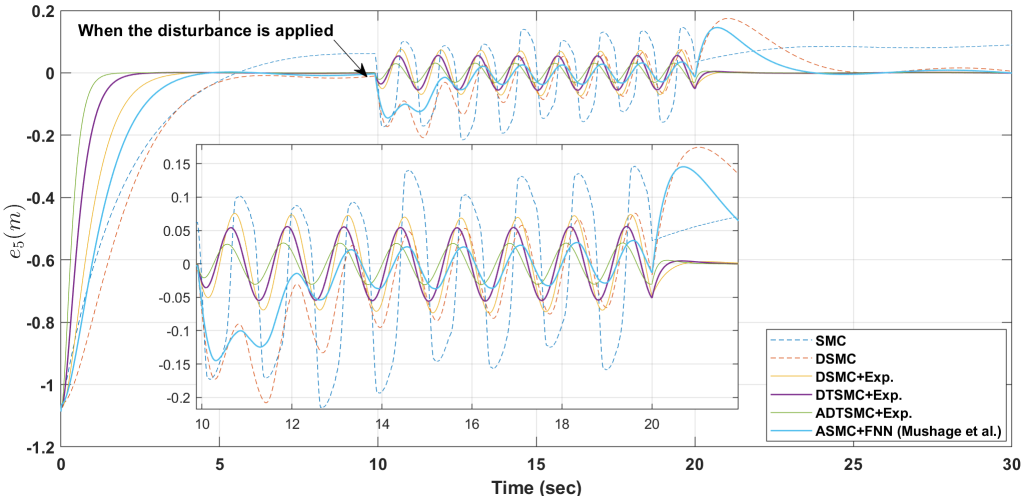

Figure 15. The error trajectory of e_5 using the SMC, DSMC, DSMC with exponential term, DTSMC with exponential term, ADTSMC with exponential term, and ASMC with FNN [27] in the second example.

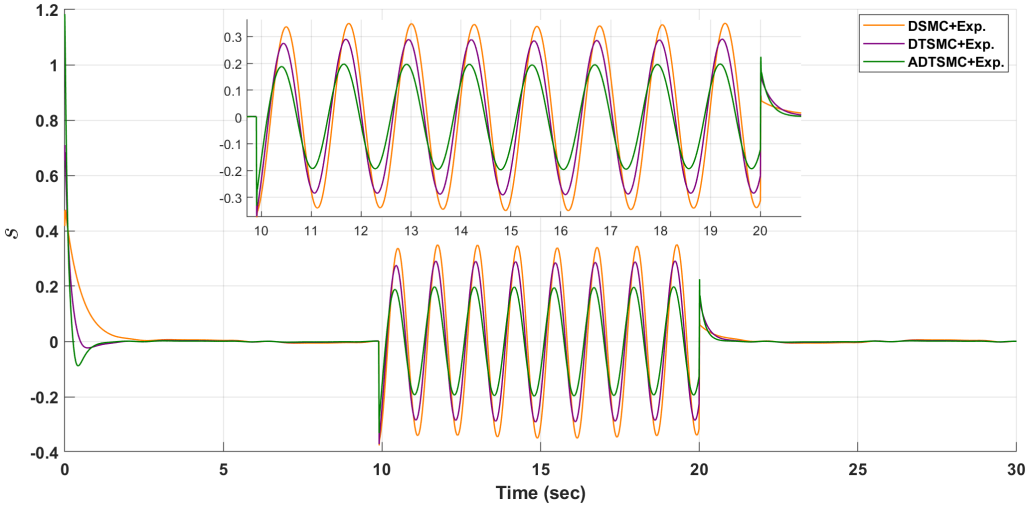

Figure 16. The first sliding surface (s) in the DSMC with exponential term, DTSMC with exponential term, and ADTSMC with exponential term in the second example.

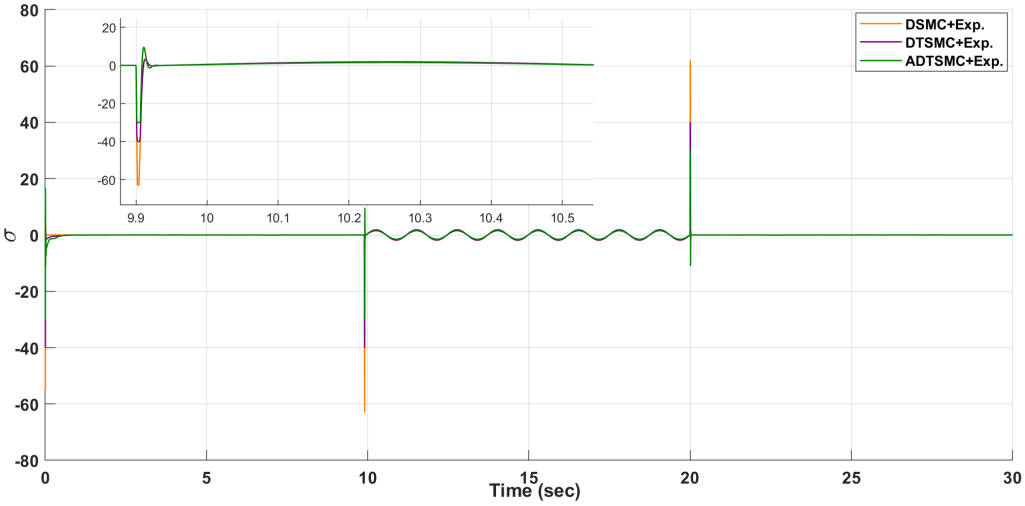

Figure 17. The second sliding surface (σ) in the DSMC with exponential term, DTSMC with exponential term, and ADTSMC with exponential term in the second example.

https://dx.doi.org/10.57647/mjee.2026.2001.05

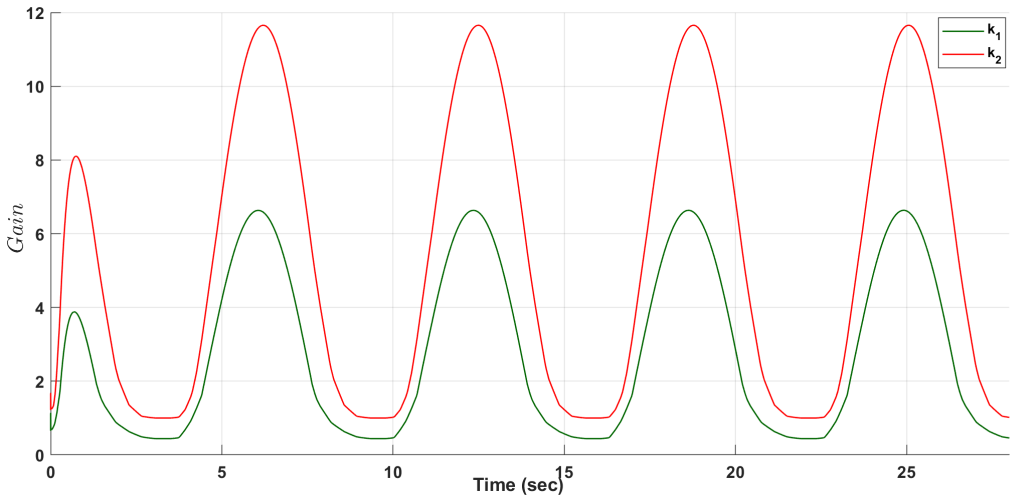

Figure 18. The adaptive control gains in ADTSMC with exponential term in the second example.

Figure 18 depicts the adaptive control gains in ADTSMC with an exponential term in the second example.

As shown in figure 18, the adaptive gains K_1 and K_2 adjust dynamically to system uncertainties and disturbances, ensuring stability and effective performance by modulating control effort based on the system's needs. Smooth transitions in the gain profiles reflect robustness, preventing instability and excessive oscillations. The adaptive control laws regulate real-time updates to the gains, slowing adaptation as the error approaches zero to prevent abrupt changes, and accelerating convergence when the error is large for precise control. These dynamic adjustments enhance system robustness and effectiveness, particularly in applications like robotics, where the system must adapt to unpredictable environments. The adaptive gains ensure stability and performance while minimizing control effort as conditions evolve.

3.3 Performance analysis of the proposed ADTSMC with exponential term

The analysis of figures 3- 18 and Tables 1 and 2 reveals that the DSMC is more effective in reducing the chattering phenomenon compared to the Standard SMC. However, it's worth noting that the dynamic sliding surface does not significantly impact the convergence rate. In contrast, the introduction of an exponential term within DSMC yields a dual benefit: It reduces both the convergence rate and the occurrence of chattering in the control signal. The utilization of a terminal sliding mode surface within the Dynamic Terminal Sliding Mode Control (DTSMC) framework notably accelerates the control system's response speed. Incorporating the ELM neural network as an adaptive intelligent system enhances performance compared to non-adaptive methods. As a result, the ADTSMC with the exponential term surpasses all previously presented strategies. The simulated results, as presented in the figures and tables, provide strong evidence of the proposed controller's robustness and ability to effectively handle bounded uncertainty and external disturbances. As demonstrated in references [30] and [31], the proposed control strategy ensures Lyapunov stability when the optimal values of the controller parameters are utilized. This finding validates the stability of the system under the derived conditions, highlighting the robustness of the control approach in addressing uncertainties and achieving reliable performance.

The statistical analysis highlights the superior performance of the ADTSMC with the exponential term, covering various aspects, including variable states such as the position and velocity of exoskeleton joints and control signals indicative of the system's ability to manipulate movements. Based on quantitative metrics, the analysis consistently shows that ADTSMC with the ex-

Table 2. Control results in the second example using the SMC, DSMC, DSMC with exponential term, DTSMC with exponential term, ADTSMC with exponential term, and ASMC with FNN [27].

Controller	ISE (m^2)	ITSE (m^2sec)	CE ((N·m)^{2}sec)	ACM (m)
SMC	27.9928	34.9739	355072.23	2.8333×10^{-1}
DSMC	27.4683	24.9798	18014.46	1.2015×10^{-1}
DSMC with exponential term	13.7801	6.2462	16452.17	4.6911×10^{-2}
DTSMC with exponential term	6.3747	1.5118	14752.64	3.9870×10^{-2}
ADTSMC with exponential term	5.214	0.888	10468.14	3.2512×10^{-2}
ASMC with FNN [27]	18.4215	11.19	188661.75	1.0072×10^{-1}

https://dx.doi.org/10.57647/mjee.2026.2001.05

ponential term outperforms alternative control strategies. This superiority extends to achieving precise trajectory tracking, optimizing convergence rates, and enhancing resilience against disturbances. Notably, lower values in these metrics are considered desirable, indicating more efficient control efforts. For example, a smaller CE signifies more efficient practical control signal, and lower values for ISE, ITSE, and ACM suggest superior trajectory tracking and reduced chattering effects. Notably, this approach even outperforms the adaptive fuzzy neural network sliding mode controller introduced by [27].

In summation, the proposed ADTSMC with the exponential term demonstrates its prowess across various scenarios. It guarantees finite-time convergence, showcases robust performance in the face of external disturbances and uncertainties, and emerges as a frontrunner in achieving control excellence.

4. Conclusion

This paper introduces a novel adaptive intelligent controller specifically designed for the position control of a 5-DOF robot. The proposed method employs an ELM enhanced with the ReLU activation function, ensuring improved controller performance by preventing entrapment in local minima. The strategy guarantees finite-time convergence, eliminates the notorious chattering phenomenon, and demonstrates robustness all substantiated through rigorous analysis. Simulation results across various scenarios highlight the proposed approach's success in addressing chattering, managing parametric uncertainties, and mitigating external disturbances. Moreover, a comparative evaluation against existing controllers in the literature validates the proposed method's efficiency and robustness.

Authors contributions
All authors contributed equally to the conception, design, execution, and writing of this work. All authors read and approved the final manuscript.

Availability of data and materials
The authors declare that the data supporting the findings of this study are available within the paper.

Conflict of interests
The authors assert that they do not have any identifiable conflicting financial interests or personal relationships that might be perceived to influence the work presented in this paper.

References

1. Rahmani M and Rahman MH. "**An upper-limb exoskeleton robot control using a novel fast fuzzy sliding mode control.**" J. Intell. Fuzzy Syst. 2019; 36:2581–92. DOI: 10.3233/JIFS-181558
2. Thogersen MB et al. "**User based development and test of the EXOTIC exoskeleton: empowering individuals with tetraplegia using a compact, versatile, 5-DoF upper limb exoskeleton controlled through intelligent semi-automated shared tongue control.**" Sensors 2022; 22:6919. DOI: 10.26634/jic.12.1.20513
3. Vaziri A and Fang H. "**Optimal Inferential Control of Convolutional Neural Networks.**" arXiv Prepr 2024. DOI: 10.48550/arXiv.2410.09663
4. Yu Z, Zhang J, and Wang X. "**Thrust Vectoring Control of a Novel Tilt-Rotor UAV Based on Backstepping Sliding Model Method.**" Sensors 2023; 23. DOI: 10.3390/s23020574
5. Labbaf-Khaniki MA, Manthouri M, and Ahmadieh-Khanesar M. "**Adaptive non-singular fast terminal sliding mode control and synchronization of a chaotic system via interval type-2 fuzzy inference system with proportionate controller.**" Iran. J. Fuzzy Syst. 2023; 20:171–85. DOI: 10.22111/IJFS.2023.39658.6889
6. Norouzi M, Zhou M, and Yuan C. "**Cooperative Deterministic Learning-Based Formation Control for a Group of Nonlinear Mechanical Systems Under Complete Uncertainty.**" arXiv Prepr 2025. DOI: 10.48550/arXiv.2503.13688
7. Norouzi M, Amirani MZ, Shahriari Y, and Abiri R. "**Precision Enhancement in Sustained Visual Attention Training Platforms: Offline EEG Signal Analysis for Classifier Fine-Tuning.**" IEEE 2024 :1–5. DOI: 10.1109/EMBC53108.2024.10782784
8. Labbaf-Khaniki MA and Tavakoli-Kakhki M. "**Adaptive type-II fuzzy nonsingular fast terminal sliding mode controller using fractional-order manifold for second-order chaotic systems.**" Asian J. Control 2022; 24:2395–409. DOI: 10.1002/asjc.2653
9. Labbaf-Khaniki MA, Salehi-Kho M, and Aliyari-Shoorehdeli M. "**Control and synchronization of chaotic spur gear system using adaptive non-singular fast terminal sliding mode controller.**" Trans. Inst. Meas. Control 2022; 44:2795–808. DOI: 10.1177/01423312221087578
10. Hou H, Yu X, Xu L, Rsetam K, and Cao Z. "**Finite-time continuous terminal sliding mode control of servo motor systems.**" IEEE Trans. Ind. Electron 2019; 67:5647–56. DOI: 10.1109/TIE.2019.2931517
11. Babaey V and Ravindran A. "**GenSQLi: A Generative Artificial Intelligence Framework for Automatically Securing Web Application Firewalls Against Structured Query Language Injection Attacks.**" Futur. Internet 2025; 17. DOI: 10.3390/fi17010008
12. Babaey V and Ravindran A. "**GenXSS: an AI-Driven Framework for Automated Detection of XSS Attacks in WAFs.**" IEEE 2025 :1519–24. DOI: 10.1109/SoutheastCon56624.2025.10971558

13. Nasri M, Kosa M, Chukoskie L, Moghaddam M, and Harteveld C. "**Exploring Eye Tracking to Detect Cognitive Load in Complex Virtual Reality Training.**" (ISMAR-Adjunct) 2024 :51–4. DOI: 10.1109/ISMAR-Adjunct64951.2024.00022

14. Labbaf-Khaniki MA, Mirzaeibonehkhater M, Samii A, and Manthouri M. "**Adaptive Control of Spur Gear Systems via Proximal Policy Optimization and Attention-Based Learning.**" (ICCIA) 2023 :1–5. DOI: 10.1109/ICCIA61416.2023.10506397

15. Jandaghi E, Stein DL, Hoburg A, Stegagno P, Zhou M, and Yuan C. "**Composite Distributed Learning and Synchronization of Nonlinear Multi-Agent Systems with Complete Uncertain Dynamics.**" (AIM), IEEE 2024 :1367–72. DOI: 10.1109/AIM55361.2024.10637197

16. Jandaghi E, Zhou M, Stegagno P, and Yuan C. "**Adaptive formation learning control for cooperative AUVs under complete uncertainty.**" Front. Robot. AI 2025; 11:1491907. DOI: 10.3389/frobt.2024.1491907

17. Ali M, Khaniki L, and Kho MS. "**Control and synchronization of chaotic spur gear system using adaptive non-singular fast terminal sliding mode controller.**" 2022. DOI: 10.1177/01423312221087578

18. Nasri M et al. "**Designing a Virtual Reality Training Apprenticeship for Cold Spray Advanced Manufacturing.**" (ISMAR-Adjunct), IEEE 2024 :541–4. DOI: 10.1109/ISMAR-Adjunct64951.2024.00156

19. Vaziri A, Askari I, and Fang H. "**Bayesian Inferential Motion Planning Using Heavy-Tailed Distributions.**" arXiv Prepr 2025. DOI: 10.48550/arXiv.2503.22030

20. Ghajari G, Ghajari E, Mohammadi H, and Amsaad F. "**Intrusion Detection in IoT Networks Using Hyperdimensional Computing: A Case Study on the NSL-KDD Dataset.**" arXiv Prepr 2025. DOI: 10.48550/arXiv.2503.03037

21. Ghajari G, Ghimire A, Ghajari E, and Amsaad F. "**Network Anomaly Detection for IoT Using Hyperdimensional Computing on NSL-KDD.**" arXiv Prepr 2025. DOI: 10.48550/arXiv.2503.03031

22. Shahin M, Chen FF, Maghanaki M, Firouzranjbar S, and Hosseinzadeh A. "**Evaluating the fidelity of statistical forecasting and predictive intelligence by utilizing a stochastic dataset.**" Int. J. Adv. Manuf. Technol. 2024 :1–31. DOI: 10.1007/s00170-024-14505-8

23. Safari K, Safari A, and Manthouri M. "**Designing an Adaptive-Intelligent Controller for Quadcopter Based on Brain Emotional Learning.**" (ICCIA), IEEE 2023 :1–5. DOI: 10.1109/ICCIA61416.2023.10506364

24. Ostovar A, Davari DD, and Dzikuc M. "**Determinants of Design with Multilayer Perceptron Neural Networks: A Comparison with Logistic Regression.**" Sustainability 2025; 17:2611. DOI: 10.3390/su17062611

25. Safari K, Rodriguez-Vila B, and Pierce DM. "**Automated Detection of Microcracks Within Second Harmonic Generation Images of Cartilage Using Deep Learning.**" J. Orthop. Res. 2025. DOI: 10.1002/jor.26071

26. Ahmadirad Z. "**The role of AI and machine learning in supply chain optimization.**" Int. J. Mod. Achiev. Sci. Eng. Technol. 2025; 2:1–8. DOI: 10.63053/ijset.77

27. Mushage BO, Chedjou JC, and Kyamakya K. "**Fuzzy neural network and observer-based fault-tolerant adaptive nonlinear control of uncertain 5-DOF upper-limb exoskeleton robot for passive rehabilitation.**" Nonlinear Dyn. 2017; 87:2021–37. DOI: 10.1007/s11071-016-3173-7

28. Kang HB and Wang JH. "**Adaptive control of 5 DOF upper-limb exoskeleton robot with improved safety.**" ISA Trans. 2013; 52:844–52. DOI: 10.1016/j.isatra.2013.05.003

29. Bin-Huang G, Zhu QY, and Siew C. "**Extreme learning machine: Theory and applications.**" Neurocomputing 2006; 70:489–501. DOI: 10.1016/j.neucom.2005.12.126

30. Zhang Y, Guo J, and Xiang Z. "**Finite-Time Adaptive Neural Control for a Class of Nonlinear Systems With Asymmetric Time-Varying Full-State Constraints.**" IEEE Trans. Neural Networks Learn. Syst. 2022. DOI: 10.1109/TNNLS.2022.3164948

31. Dheeraj K, Jacob J, and Nandakumar M. "**Direct adaptive neural control design for a class of nonlinear multi input multi output systems.**" IEEE Access 2019; 7:15424–35. DOI: 10.1109/ACCESS.2019.2892460